On the Effect of Plastic Spin on Large Strain Elastic-Plastic Torsion of Solid Bars

Giessen, E. van der; Wu, P.D.; Neale, K.W.

Published in:
International Journal of Plasticity

DOI:
10.1016/0749-6419(92)90002-T

Publication date:
1992

International Journal of Plasticity, Vol. 8, pp. 773–801, 1992
Printed in the USA

0749-6419/92 $5.00 + .00

ON THE EFFECT OF PLASTIC SPIN ON LARGE STRAIN ELASTIC-PLASTIC TORSION OF SOLID BARS

E. VAN DER GIESSEN,* P.D. WU,** and K.W. NEALE†

*Delft University of Technology,
**China University of Mining and Technology,† Université de Sherbrooke

(Communicated by Kerry Havner, North Carolina State University)

Abstract—The plastic spin has recently been identified as a key concept in the macroscopic description of large deformation plasticity for the treatment of anisotropic hardening. A class of combined isotropic-kinematic hardening models is formulated here, which includes two alternative constitutive equations for the plastic spin. The various sets of constitutive equations are used to analyze the large strain torsion of solid circular bars with either axially fixed ends or free ends. These analyses are carried out numerically using special purpose finite elements and, when feasible for particular cases, by means of a semianalytical method. It is shown that the plastic spin, and its different constitutive descriptions, have a significant influence on the predicted torque response and, in particular, on the axial Swift effects. The differences between fixed-end and free-end predictions are emphasized. It is found that the difference in predicted axial effects for the various plastic spin constitutive laws is most pronounced in fixed-end torsion, while the torque response is most sensitive in free-end torsion.

I. INTRODUCTION

Modeling deformation-induced anisotropy during large strain elastoplastic deformation processes has been a longstanding subject in the field. Kinematic hardening, possibly with simultaneous isotropic hardening, has been rather popular as a first simplistic representation of anisotropic hardening. In many large strain plasticity studies, the motivation for using a kinematic hardening model has been to account in an approximate way for the presence of a small radius of curvature of the yield surface at the loading point (see e.g. TVERGAARD [1978]; MEAR & HUTCHINSON [1985]). The recognition (NAGTEGAAL & DEJONG [1982]) of an unrealistic response in simple shear according to the finite strain generalization of kinematic hardening due to TVERGAARD [1978] has given a new impulse to work in this area. Important advances have been made since, not in the least in constitutive theories based upon the framework set up by MANDEL [1971]. In particular, it has been recognized that the concept of *plastic spin* appearing in this framework plays a key role in the description of the evolution of anisotropy. This leads to the introduction of a particular stress rate which involves corotation at a rate determined by the continuum spin as well as the plastic spin.

For kinematic hardening, DAFALIAS [1983,1985a,b] and LORET [1983] were the first to propose specific constitutive laws for the plastic spin through a tensor function of Cauchy stress and a symmetric back stress. Their argument was based on tensor representation theorems, while a micromechanical motivation was given subsequently by AIFANTIS [1987]. Other contributions along these lines are from, e.g., PAULUN and PECHERSKI [1987a,b].

A different approach was initiated in 1987 by this study's first author (VAN DER GIESSEN [1990]), based upon an extension of the framework by the concept of a plastically

induced orientation structure (PIOS). This PIOS is introduced to explicitly incorporate the presence and development of texture into the continuum model in some phenomenological manner. In a natural way, this theory leads to *nonsymmetric* tensorial internal state variables, which, in turn, govern the plastic spin through a generalized normality condition. A large deformation kinematic hardening model emerges from the theory as a special case (VAN DER GIESSEN [1989b]). A critical discussion of the various proposals for plastic spin constitutive laws in the light of the thermodynamics of plasticity and invoking micromechanical considerations is given in VAN DER GIESSEN [1991].

The analysis of simple shear deformations has become a popular benchmark for testing the appropriateness of large strain constitutive equations. In principle, simple shear can be produced approximately by torsion of thin-walled tubes with the ends prevented to displace in the axial direction. Comparisons between predictions of the constitutive theories referred to above and such experiments have been carried out (see e.g. PAULUN & PECHERSKI [1987a]; ZBIB & AIFANTIS [1988]); but buckling at large twists poses a serious experimental difficulty, while it has also been reported that it is notoriously difficult to actually create a homogeneous state of simple shear in such specimens (e.g. LIPKIN *et al.* [1988]). Torsion of a relatively long bar with a solid circular cross-section leads to a much more homogenous state of deformation along the longitudinal axis of the specimen and, therefore, seems to offer significant experimental advantages. However, the dependence on the radial coordinate is essential and complicates the analysis. In a series of papers, NEALE and SHRIVASTAVA [1985,1990a] developed a semianalytical method for the analysis of torsion of solid bars of incompressible material under fixed-end conditions. Very recently it was shown that a closed-form analytical solution may be given when the analytical solution of the simple shear problem is available (NEALE & SHRIVASTAVA [1990b]). Torsion with the ends free to displace axially may be even more convenient from an experimental point of view, but the analysis is significantly more involved. For this purpose, WU and VAN DER GIESSEN [1991] presented a numerical approach based on a simple but effective dedicated finite element, which is suited for free-end conditions as well as fixed-end and intermediate conditions.

Of particular importance is the axial or "Swift" effect; i.e. the development of significant axial strains during free-end torsion (SWIFT [1947]), or the development of axial forces during fixed-end torsion. It has been established that these axial effects at large plastic torsional strains are mainly due to texture in the polycrystalline material (e.g. GIL-SEVILLANO *et al.* [1975], HARREN *et al.* [1989]). The axial effects at elevated temperatures are of a more complex nature (see e.g. MONTHEILLET *et al.* [1984]), but we shall not consider that here. Therefore, the axial effects seem to provide a suitable means for assessing the adequacy of macroscopic constitutive models which aim at describing deformation-induced anisotropy. Indeed, the prediction of the axial effects shows a remarkably strong dependence on the constitutive relation adopted: isotropic hardening predicts virtually no axial effect (NEALE & SHRIVASTAVA [1985]), while kinematic hardening tends to overestimate the axial effects, but this is strongly dependent on the precise formulation (e.g. NEALE & SHRIVASTAVA [1990b]; WU & VAN DER GIESSEN [1991]). Case studies of simple shear by DAFALIAS [1985a]; LORET [1983], and others indicated that this pertains also to details of the constitutive description of the plastic spin.

In this study, we therefore perform a detailed study of the effect of plastic spin during large strain torsion of solid bars, focusing especially on axial effects. The aim of this work is to present some principal predictive features of various plastic spin constitutive laws and differences in trends between fixed-end and free-end torsion. This insight will thus contribute to the further development of appropriate plastic spin constitutive laws

on the basis of torsion experiments. We shall start by presenting two competitive sets of constitutive equations for kinematic hardening combined with isotropic hardening, which differ mainly in the plastic spin laws used and, associated with that, the evolution relations of the back stress. One of these sets is based on the plastic spin constitutive law initially by DAFALIAS [1983,1985a,b] and LORET [1983], the other is based on the work of VAN DER GIESSEN [1989b], both including slight modifications. The constitutive relations are designed such that they coincide for proportional stress histories. In addition we present an alternative combined isotropic-kinematic hardening model using the fraction model concept (BESSELING [1958]). The analysis of large strain torsion of solid bars is carried out numerically using the above-mentioned finite element technique and, for fixed-end torsion, by means of the semianalytical method, so as to assess the accuracy of the numerical method.

Tensors are denoted by boldface letters. The tensor product is denoted by $\otimes$ and the following operations apply: $\mathbf{ab} = a^{ik}b_{kj}\mathbf{g}_i \otimes \mathbf{g}^j$, $\mathbf{a} : \mathbf{b} = a^{ij}b_{ij}$, with proper extension to higher-order tensors. Here, $\{\mathbf{g}_i\}$ and $\{\mathbf{g}^i\}$ are reciprocal bases associated with a spatially fixed curvilinear coordinate system, with metric coefficients g_{ij} and g^{ij}. Superscripts T and -1 denote the transverse and inverse of a second-order tensor, respectively, tr denotes the trace, and a superposed dot denotes the material time derivative or rate.

II. CONSTITUTIVE EQUATIONS

Isotropic hardening and kinematic hardening may be regarded as representing two traditional extreme models for the actual hardening behavior. Kinematic hardening models have been used in many large strain studies merely for the reason that they provide a first, very simple model for deformation-induced anisotropy. In effect, it gives important insight in the effect of the small radius of curvature of the yield surface at the loading point (see e.g. TVERGAARD [1978]; MEAR & HUTCHINSON [1985]). It must be realized though that the actual behavior is usually much more involved; but for deformation processes that do not deviate much from proportional deformation paths, a combination of isotropic and kinematic hardening may give a reasonable approximation of the actual behavior.

In this section, we start out by recapitulating some general expressions, mainly for the purpose of notation. Then we proceed to develop two combined isotropic-kinematic hardening models based upon two different plastic spin constitutive laws: one based on the work of DAFALIAS [1983,1985a,b] and LORET [1983] (referred to in the sequel as the DL model) and the other based on VAN DER GIESSEN [1989b] (the VDG model). We conclude with a fraction or overlay model with similar hardening characteristics.

II.1. *General aspects*

The notion of an intermediate configuration is now well-established in the field of large strain plasticity, although precise definitions may differ (see e.g. DAFALIAS [1987]; VAN DER GIESSEN [1989a]). In any case, such concepts lead to the kinematic decomposition of the velocity gradient $\mathbf{L}$ in elastic (e) and plastic (p) parts,

$$\mathbf{L} = \mathbf{L}^e + \mathbf{L}^p, \quad \text{or } \mathbf{D} = \mathbf{D}^e + \mathbf{D}^p, \quad \mathbf{W} = \mathbf{W}^e + \mathbf{W}^p. \tag{1}$$

Here, $\mathbf{D}^{(\,)}$ and $\mathbf{W}^{(\,)}$ denote the strain-rate and spin parts of $\mathbf{L}^{(\,)}$, respectively. Although the precise definition of the various tensors may differ, the tensor $\mathbf{W}^e$ represents the

spin due to the rate of elastic distortion along with the spin of the embedded directions of anisotropy or so-called substructure, while $\mathbf{W}^p$ mainly represents the spin of the material relative to this substructure caused by the plastic deformation process. MANDEL [1971] was the first to explicitly put forward that a complete constitutive theory requires not only constitutive equations for the plastic strain-rate $\mathbf{D}^p$, but also for the plastic spin $\mathbf{W}^p$. In section II.2, we consider two sets of such constitutive equations based on earlier work by DAFALIAS [1983,1985a,b]; LORET [1983]; and VAN DER GIESSEN [1989b].

In this study, we will assume that the elastic response is governed by the following hypoelastic-type rate equation:

$$\check{\boldsymbol{\sigma}} = \mathfrak{L} : \mathbf{D}^e, \tag{2}$$

with the usual tensor of elastic moduli

$$\mathfrak{L} = \mathfrak{L}^{ijkl}\mathbf{g}_i \otimes \mathbf{g}_j \otimes \mathbf{g}_k \otimes \mathbf{g}_l, \quad \mathfrak{L}^{ijkl} = \frac{E}{1+\nu}\left[\frac{1}{2}(g^{ik}g^{jl} + g^{il}g^{jk}) + \frac{\nu}{1-2\nu}g^{ij}g^{kl}\right], \tag{3}$$

(E is Young's modulus, ν is Poisson's ratio) and where the stress-rate is defined as

$$\check{\boldsymbol{\sigma}} = \dot{\boldsymbol{\sigma}} - \mathbf{W}^e\boldsymbol{\sigma} + \boldsymbol{\sigma}\mathbf{W}^e. \tag{4}$$

These expressions can be readily obtained from the hyperelastic rate equations derived by, e.g., LORET [1983] and VAN DER GIESSEN [1989a], by invoking the assumption of small elastic strains. Using (1) to rewrite (2) in terms of the Jaumann stress rate,

$$\mathring{\boldsymbol{\sigma}} = \dot{\boldsymbol{\sigma}} - \mathbf{W}\boldsymbol{\sigma} + \boldsymbol{\sigma}\mathbf{W},$$

we obtain

$$\mathring{\boldsymbol{\sigma}} = \mathfrak{L} : (\mathbf{D} - \mathbf{D}^p) - \mathbf{W}^p\boldsymbol{\sigma} + \boldsymbol{\sigma}\mathbf{W}^p. \tag{5}$$

Using the plastic flow rule to be specified later, the plastic strain-rate $\mathbf{D}^p$ can be expressed in terms of the strain-rate $\mathbf{D}$. Furthermore, by eliminating the plastic spin $\mathbf{W}^p$ from (5) by invoking its constitutive law, the rate equations for $\boldsymbol{\sigma}$ can be written in the general form

$$\mathring{\boldsymbol{\sigma}} = [\mathfrak{L} - (1-h)\mathfrak{Y}] : \mathbf{D} \tag{6}$$

in terms of the plastic modulus tensor $\mathfrak{Y}$, which depends on the flow rule and the plastic spin constitutive law, and a hardening parameter h, which will be determined from the uniaxial stress–strain curve. Here, the uniaxial true stress–logarithmic strain curve is taken to be represented by the piecewise power law

$$\frac{\sigma}{\sigma_y} = \begin{cases} \dfrac{E}{\sigma_y}\varepsilon & \text{if } \sigma \le \sigma_y \\ \left(\dfrac{E}{\sigma_y}\varepsilon\right)^N & \text{if } \sigma \ge \sigma_y \end{cases} \tag{7}$$

where σ_y is the initial yield stress and N is the strain-hardening exponent.

II.2. *Combined isotropic-kinematic hardening models*

In a combined isotropic-kinematic hardening model the yield surface not only changes in size, but also translates in stress-space during plastic deformation. The current yield condition is of the form

$$\Phi(\bar{\mathbf{s}}) = \text{const}$$

where $\bar{\mathbf{s}}$ is defined by

$$\bar{\mathbf{s}} = \frac{1}{H}(\mathbf{s} - \mathbf{a}) \tag{8}$$

in terms of Cauchy's stress deviator $\mathbf{s} = \boldsymbol{\sigma} - \frac{1}{3}(\text{tr}\,\boldsymbol{\sigma})\mathbf{I}$, the back stress $\mathbf{a}$ which specifies the translation of the yield surface center in stress space, and a hardening parameter H, which specifies the expansion of the yield surface ($H = 1$ corresponds to pure kinematic hardening). When a Mises type yield surface is assumed, the yield condition is given by

$$\Phi = \tfrac{3}{2}\text{tr}\,\bar{\mathbf{s}}^2 = \sigma_y^2, \tag{9}$$

where σ_y is the initial yield stress. In this formulation, the current radius of the yield surface, or the flow stress σ_F, is $H\sigma_y$. Following MEAR and HUTCHINSON [1985], we take this radius to be given by

$$\sigma_F \equiv H\sigma_y = (1 - b)\sigma_y + b\sigma_e \tag{10}$$

where $\sigma_e = \sqrt{3\,\text{tr}\,\mathbf{s}^2/2}$ is the current value of the effective Mises stress and where the parameter b is a constant in the range [0,1]. Purely isotropic behavior is obtained for $b = 1$, while pure kinematic hardening corresponds to $b = 0$. Furthermore, the stress σ to be substituted into (7) for the evaluation of h is taken as σ_e.

With these assumptions, the final rate equations for the Cauchy stress can be cast in the form (6) with the tensor $\mathfrak{Y}$ being of the form

$$\mathfrak{Y} = \frac{1}{\zeta}\mathbf{M}_G \otimes \mathbf{M}_F. \tag{11}$$

The second-order tensors, $\mathbf{M}_G$ and $\mathbf{M}_F$, depend on the constitutive equations for plastic strain-rate and plastic spin. It is noted that if these tensors are not identical, the tensor $\mathfrak{Y}$ and, hence, the total modulus tensor do not possess the symmetry properties that are necessary for application of HILL's [1958] extremum principles and uniqueness theorems.

II.2.1. *The DL model.* The kinematic hardening model proposed by DAFALIAS [1983,1985a,b] and LORET [1983] uses an associated flow rule for the plastic strain-rate $\mathbf{D}^p$, supplemented with a separate tensor equation for the plastic spin $\mathbf{W}^p$. Similarly, for the isotropic-kinematic hardening yield function according to (9), this yields,

$$\mathbf{D}^p = \lambda\bar{\mathbf{s}}, \quad \mathbf{W}^p = \lambda\boldsymbol{\Omega}^p, \tag{12}$$

with $\boldsymbol{\Omega}^p$ defined by

$$\boldsymbol{\Omega}^p = \tfrac{1}{2}\bar{\rho}(\mathbf{a}\bar{\mathbf{s}} - \bar{\mathbf{s}}\mathbf{a}), \tag{13}$$

and where $\lambda = 0$ for elastic (un)loading and $\lambda > 0$ for plastic loading such that the consistency condition $\dot{\Phi} = 0$ is satisfied.

The parameter $\bar{\rho}$ in the plastic spin function (13) appears as an additional material function which would have to be determined from experiments; but the information available on this in the literature is very limited. Performing some case studies for pure kinematic hardening, $b = 0$, DAFALIAS [1985a] and LORET [1983] considered cases where $\bar{\rho}$ is taken to be given by a constant value ρ for simplicity. Generalizing this to combined kinematic-isotropic hardening, we shall use here either exactly the same procedure, i.e. $\bar{\rho} = \rho$ independent of b (as in TVERGAARD & VAN DER GIESSEN [1991]), or a slightly different choice where

$$\bar{\rho} = \frac{\rho}{1 - b} \,. \tag{14}$$

In the latter case, $\bar{\rho} = \rho$ in the limit of $b = 0$, while for increasing b the effective value $\bar{\rho}$ to be substituted into (13) increases. An appropriate limiting procedure has to be applied when $b \to 1$ in order that $\mathbf{\Omega}^p \to \mathbf{0}$ as required for pure isotropic hardening. A heuristic motivation for this modified expression will be given in section II.3. Alternatively, PAULUN and PECHERSKI [1987a,b] proposed various expressions for $\bar{\rho}$ in terms of quantities describing the current plastic state. Here, we shall consider the expression (PAULUN & PECHERSKI [1987b])

$$\bar{\rho} = \sqrt{\frac{3}{2}} \frac{12 a_e}{h_a^2 + 3a_e^2} \tag{15}$$

in terms of the effective back stress $a_e = \sqrt{3 \operatorname{tr} \mathbf{a}^2/2}$ and a hardening factor, h_a, which is given by $h_a = EE_t/(E - E_t)$ in terms of Young's modulus E and the tangent modulus $E_t = \partial\sigma/\partial\varepsilon$ of the stress–strain curve (6). It is noted that PAULUN and PECHERSKI [1987b] assumed h_a to be related only to the kinematic hardening, while here we take it to be related to the total hardening. Yet another expression for $\bar{\rho}$ was proposed by AIFANTIS [1987] on the basis of microscopic considerations, but we shall not consider this here.

Following again DAFALIAS [1985a] and LORET [1983], the evolution equation for the back stress $\mathbf{a}$ is taken to be given by a Prager–Ziegler type shift rule,

$$\check{\mathbf{a}} = \mu \mathbf{D}^p = k\bar{\mathbf{s}}, \tag{16}$$

with the same stress rate based on $\mathbf{W}^e$, eqn (4), as in the expression (2) for the Cauchy stress rate. The parameter μ describes the kinematic hardening and is determined here by the value of the parameter b along with the total hardening specified by h. The parameter k in the last equality in (16) is found as $k = \lambda\mu$ by virtue of (12a). It is important to note here that the back stress $\mathbf{a}$ and, as a consequence, $\bar{\mathbf{s}}$ are a priori assumed to be symmetric tensors.

Using expressions (3), (5), (10), (12), (13), and (16), the value of λ follows from the consistency relation $\dot{\Phi} = 0$ after some lengthy algebra. Ultimately, the constitutive equations are fully specified by the following additional expressions:

$$\lambda = (1 - h) \frac{\mathbf{M}_F : \mathbf{D}}{\mathbf{M}_F : \bar{\mathbf{s}}}, \qquad k = h\mathbf{M}_F : \mathbf{D} - \dot{H}; \tag{17}$$

$$\mathbf{M}_F = \frac{3}{2}\frac{\mathfrak{L}:\bar{\mathbf{s}}}{\sigma_y^2} = \frac{3}{2}\frac{E}{1+\nu}\frac{\bar{\mathbf{s}}}{\sigma_y^2}, \tag{18a}$$

$$\mathbf{M}_G = \frac{3}{2\sigma_y^2}[\mathfrak{L}:\bar{\mathbf{s}} + (\boldsymbol{\Omega}^p\boldsymbol{\sigma} - \boldsymbol{\sigma}\boldsymbol{\Omega}^p)], \tag{18b}$$

$$\zeta = \frac{3}{2}\frac{\mathbf{M}_F:\bar{\mathbf{s}}}{\sigma_y^2}. \tag{19}$$

Notice that, in this model, $\mathbf{M}_G \neq \mathbf{M}_F$, so that $\mathfrak{Y}$ is not symmetric. It was already noted by DAFALIAS [1985a] in a more general discussion that the terms with $\boldsymbol{\Omega}^p$ in (18b) may be neglected when terms of the order stress/elastic moduli are neglected compared to unity, as may be allowed in the case of small elastic strains. If this is done, $\mathbf{M}_G = \mathbf{M}_F$ and $\mathfrak{Y}$ becomes symmetric. Moreover, the rate eqns (6) for the Cauchy stress become instantaneously independent of plastic spin; but of course the plastic spin remains essential in the shift rule (16). To avoid inaccuracies, the terms with $\boldsymbol{\Omega}^p$ in (18b) have been retained in the analyses carried out here.

II.2.2. *The VDG model.* Within the theoretical framework presented by VAN DER GIESSEN [1990], constitutive equations for the plastic strain-rate and the plastic spin are taken to be given through a generalized associated flow rule for $\mathbf{L}^p$. For the yield function given by (9), this yields

$$\mathbf{L}^p = \lambda\bar{\mathbf{s}}^T. \tag{20}$$

Here we have carefully allowed for the fact that $\bar{\mathbf{s}}$ may be a nonsymmetric tensor when the tensor $\mathbf{a}$, which specifies the translation of the yield surface center, is nonsymmetric. In the case of a symmetric tensor $\bar{\mathbf{s}}$, the plastic spin vanishes according to (20), whereas, in the case of a nonsymmetric tensor $\mathbf{a}$, the plastic spin is completely determined by the antisymmetric part,

$$\mathbf{D}^p = \lambda\bar{\mathbf{s}}_{\text{symm}}, \qquad \mathbf{W}^p = \frac{\lambda}{H}\mathbf{a}_{\text{skew}}.$$

In fact, VAN DER GIESSEN [1989a,1990,1991] has put forward several arguments that would lead to concluding that if the plastic spin is relevant for a particular material, the constitutive description should include nonsymmetric internal state variables. We shall not discuss these matters further here, but we will take a pragmatic standpoint in that we shall regard this approach as a valid alternative to the approach discussed in the previous section.

Following the development in VAN DER GIESSEN [1990], the tensor $\mathbf{a}$ is defined as

$$\mathbf{a} = H\mathbf{m},$$

in terms of the so-called microstress tensor $\mathbf{m}$. For kinematic hardening, $H = 1$, an evolution equation for $\mathbf{m}$ was proposed within the PIOS framework (VAN DER GIESSEN [1989b]). For the present combined isotropic–kinematic hardening model we use the following slightly modified expression:

$$\mathring{\mathbf{m}} = \frac{\mu}{H}\mathbf{L}^{pT} - \frac{\dot{H}}{H}\mathbf{m}, \tag{21}$$

where the objective microstress rate is defined by

$$\mathring{\mathbf{m}} = \dot{\mathbf{m}} - \mathbf{m}\mathbf{L}^T + \mathbf{L}^T\mathbf{m}. \tag{22}$$

As compared with VAN DER GIESSEN [1989b], we have neglected a term in the definition of $\mathring{\mathbf{m}}$ involving tr $\mathbf{D}$; this represents the dilatation rate, which, in this model, is due only to elastic effects which are assumed to be small. In (21) we have added the isotropic hardening term with $\dot{H}$ so that the rate equation for $\mathbf{a}$ becomes

$$\mathring{\mathbf{a}} = \mu\mathbf{L}^{pT} = k\bar{\mathbf{s}}. \tag{23}$$

This expression is similar in form to (16), but involves a different stress rate and includes an additional contribution from the plastic spin in the second member. It is essential to note that as a consequence of this and along with the particular stress rate $\mathring{\mathbf{a}}$ [cf. (22)], the back stress $\mathbf{a}$ will in general develop into a nonsymmetric tensor, the skew-symmetric part of which defines the direction of plastic spin as discussed above.

The parameter λ in (20) is derived from the consistency relation $\dot{\Phi} = 0$ as before. Skipping the derivation, λ and k are given again by the expressions (17), ζ is given again by (19), but $\mathbf{M}_G$ and $\mathbf{M}_F$ are now defined by

$$\mathbf{M}_G = \mathbf{M}_F = \frac{3}{2}\frac{\mathfrak{L}_0^* : \bar{\mathbf{s}}^T}{\sigma_y^2} = \frac{3}{2}\frac{\bar{\mathbf{s}}^T : \mathfrak{L}_0}{\sigma_y^2}, \tag{24}$$

instead of by (18). Here, the tensors $\mathfrak{L}_0$ and $\mathfrak{L}_0^*$ are defined by

$$\mathfrak{L}_0 = \mathfrak{L}_0^{ijkl}\mathbf{g}_i \otimes \mathbf{g}_j \otimes \mathbf{g}_k \otimes \mathbf{g}_l, \qquad \mathfrak{L}_0^* = \mathfrak{L}_0^{*ijkl}\mathbf{g}_i \otimes \mathbf{g}_j \otimes \mathbf{g}_k \otimes \mathbf{g}_l$$

$$\mathfrak{L}_0^{*ijkl} = \mathfrak{L}_0^{klij}, \qquad \mathfrak{L}_0^{ijkl} = \mathfrak{L}^{ijkl} + \tfrac{1}{2}(g^{il}\sigma^{jk} + g^{ik}\sigma^{jl} - g^{jl}\sigma^{ik} - g^{jk}\sigma^{il}).$$

Note that $\mathfrak{L}_0^{ijkl}$ is symmetric in its last and $\mathfrak{L}_0^{*ijkl}$ in its first two indices, so that $\mathbf{M}_G$ and $\mathbf{M}_F$ are symmetric tensors as required by the intrinsic symmetry of $\mathbf{D}$ and $\boldsymbol{\sigma}$ [cf. (6)]; but $\mathfrak{L}_0^{ijkl}$ is not symmetric in the first two indices, which agrees with the nonsymmetry of $\bar{\mathbf{s}}$. Also, note that $\mathfrak{Y}$ is an essentially symmetric tensor in this model because $\mathbf{M}_G$ and $\mathbf{M}_F$ are identical (see also VAN DER GIESSEN [1989b]).

It is finally noted that the DL and VDG models presented here coincide for proportional stressing, i.e. in cases where the principal directions of stress remain fixed in space during the deformation process. In that case the plastic spin vanishes in both models and the microstress $\mathbf{m}$ reduces to a symmetric tensor. In fact, all combined isotropic-kinematic hardening models based on the rate eqns (2) and (16), but involving different spins in the definition of the ($\check{}$) stress rate, coincide in this case.

II.3. *The fraction model*

The fraction or overlay model originally designed by BESSELING [1958] has been shown very successful in the description of deformation-induced anisotropy in the range of

small elastic-plastic strains (see e.g. BESSELING [1985]). The model has been motivated by the fact that for small strains the induced anisotropy, including the Bauschinger effect, arises primarily from the fact that plastic deformations are spatially heterogeneous on a small scale. It is not entirely clear if finite strain extensions of the fraction model are adequate for describing the deformation-induced anisotropy development during large strain plastic deformation processes, since this is mainly due to other mechanisms. Nevertheless, as a phenomenological model, it is worth exploring. In fact, large strain fraction models have been applied for the analysis of metal forming processes (HUETINK [1986]), while it was also shown that large strain kinematic hardening could be described by adding one purely (hyper) elastic fraction (VAN DER GIESSEN [1985], HUETINK [1986]). Here, we shall briefly explore the characteristics of a fraction model based on the two combined hardening models discussed in the previous section and, in particular, the description of plastic spinning thus obtained.

In the fraction model, the material is conceived to be a mixture of a limited number, M, of different subelements or material fractions. Each fraction K ($K = 1, \ldots, M$) is regarded as a distinct thermomechanical system, characterized by its volume fraction Ψ_K,

$$\sum_{K=1}^{M} \Psi_K = 1,$$

the Cauchy fraction stress $\boldsymbol{\sigma}_K$ and other proper internal state variables. All fractions are subjected to the same imposed velocity gradient $\mathbf{L}$, while the macroscopic applied stress $\boldsymbol{\sigma}$ is obtained as a weighted average, $\boldsymbol{\sigma} = \sum \Psi_K \boldsymbol{\sigma}_K$. For each individual fraction, the constitutive eqns (6) are taken to apply, so that the overall constitutive equations read

$$\overset{\nabla}{\boldsymbol{\sigma}} = \sum_{K=1}^{M} \Psi_K [\mathfrak{L}_K - (1 - h_K)\mathfrak{Y}_K] : \mathbf{D}. \tag{25}$$

Although the imposed strain-rate $\mathbf{D}$ is identical for each fraction, the plastic strain-rate $\mathbf{D}_K^p$, as well as the fraction back stress $\mathbf{a}_K$, will generally be different for each fraction. It follows also that the plastic spin $\mathbf{W}_K^p$ will be different for each fraction, though they are all subjected to the same continuum spin $\mathbf{W}$. This is a consequence of the fact that each fraction is considered a distinct thermodynamic system with its own substructure, evolving according to its own constitutive equations. It is appropriate now to define an average substructure and, hence, an average plastic spin as

$$\overline{\mathbf{W}}^p = \frac{1}{\Psi^*} \sum_{K=1}^{M^*} \Psi_K \mathbf{W}_K^p, \qquad \Psi^* = \sum_{K=1}^{M^*} \Psi_K. \tag{26}$$

Here, the summation is taken to run only over the M^* anisotropic fractions ($M^* \leq M$) in which plastic spinning takes place. Isotropic fractions in which $\mathbf{W}_K^p \equiv 0$ are excluded in (26).

As an application of the fraction model approach, we consider here a model consisting of two fractions: one fraction shows pure isotropic hardening, the other is taken to show kinematic hardening according to either the DL or the VDG model emerging from the models discussed in section II.2 by letting $b = 0$. The volume fraction of the isotropic fraction is taken to be $\Psi_1 = \psi$, so that the volume fraction of the kinematic hardening fraction is $\Psi_2 = 1 - \psi$. For convenience, we take the elastic properties of the two

fractions to be identical, so that $\mathfrak{L}_K \equiv \mathfrak{L}$ in(25); but the plastic properties, i.e., the yield stress σ_y and the hardening parameter N (or E_t, or h) may be different for the two fractions. Such a model also provides a description of combined isotropic-kinematic hardening, but is somewhat different from the two formulations discussed in section II.2. The important difference is that the fraction model is slightly more versatile, since it allows for different plastic and hardening properties of the isotropic hardening and the kinematic hardening.

In the special case that the yield stress σ_y as well as the power law exponent N are taken identical for the two fractions, the resulting fraction model becomes tantamount to either one of the combined isotropic-kinematic hardening models of section II.2; this particular model will be termed the F2 model in the sequel. The volume fraction ψ, then, is similar to the parameter b in the expression (10) for the flow stress in the models of section II.2, as illustrated in Fig. 1 for uniaxial tension. Considering the total stress response of the fraction model during unidirectional straining, we may define a fictitious overall back stress a as $a = (1 - \psi)(\sigma_2 - \sigma_y)$ and a fictitious flow stress $\sigma_F = \sigma - a$, which is then found as $\sigma_F = \psi\sigma_1 + (1 - \psi)\sigma_y$. With the mentioned presumptions, $\sigma_1 = \sigma_2 = \sigma$ during unidirectional straining, so that in this case $b = \psi$. Thus, the combined hardening models of section II.2 and the associated F2 models are fully equivalent in uniaxial tension. For more complex deformation histories, like shear or torsion, the models may lead to different descriptions.

The F2 model employing the DL formulation for the kinematic hardening fraction may now be used to motivate the modified expression (14) for $\bar{\rho}$ in the combined DL model. In the F2 model, the overall plastic spin according to (26) is simply given by $\overline{\mathbf{W}}^p = \mathbf{W}_2^p$ since plastic spinning occurs only in the second, kinematic hardening fraction, while according to eqns (12) and (13),

$$\mathbf{W}_2^p = \tfrac{1}{2}\rho(\mathbf{a}_2\mathbf{D}_2^p - \mathbf{D}_2^p\mathbf{a}_2),$$

since, for this kinematic hardening fraction, $\bar{\rho} \equiv \rho$. Next, it is noted that if we define an overall back stress $\mathbf{a}$ as a weighted average of the fraction back stresses $\mathbf{a}_K$ similar

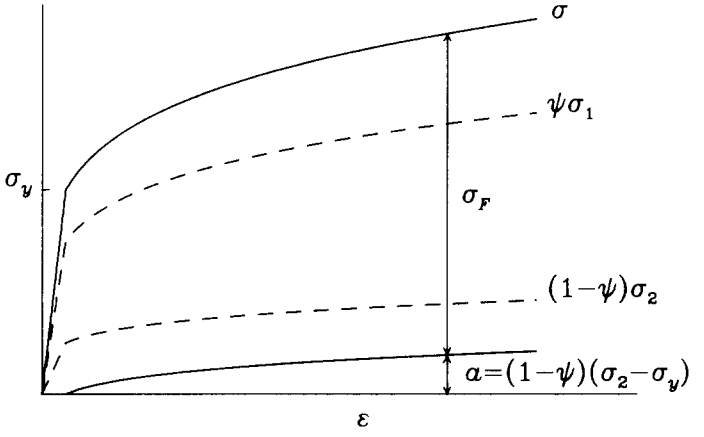

Fig. 1. Uniaxial stress strain curve for two-fraction model based on an isotropic hardening fraction of size ψ and a kinematic hardening fraction of size $1 - \psi$. The dashed curves are the contributions of the two fraction stresses. The stresses a and σ_F are the fictitious back stress and flow stress, respectively.

to the overall Cauchy stress, this back stress is in this case determined completely by the back stress $\mathbf{a}_2$ of the kinematic hardening fraction, $\mathbf{a} = (1 - \psi)\mathbf{a}_2$. The overall plastic spin may then be written as

$$\overline{\mathbf{W}}^p = \frac{1}{2}\frac{\rho}{1-\psi}(\mathbf{a}\mathbf{D}_2^p - \mathbf{D}_2^p\mathbf{a}).$$

Since $\mathbf{D}_2^p \approx \mathbf{D}$ as the elastic strains remain small, this expression is similar to the plastic spin law (12b)–(13) along with (14) for the DL combined hardening model when ψ is identified with b as above.

III. ANALYSIS OF TORSION OF SOLID BARS

III.1. *Problem formulation*

A homogeneous, solid circular bar with an initial radius R_0 and initial length L_0 is subjected to an angle of twist φ produced by an applied torque T. The lateral surface of the bar is stress-free and all properties are assumed to be axisymmetric and homogeneous along the axial direction. With the constitutive models to be used, deformation-induced anisotropy will occur, but the behavior remains axisymmetric and the bar remains circular-cylindrical with a current radius R. The end faces of the bar are constrained to the extent that they remain planar and perpendicular to the axial direction, so that we may assume that any cross-section of the bar remains plane.

Furthermore, we consider two end conditions. In the fixed-end condition, the end faces of the bar are fully constrained axially so that there is no axial displacement, thus allowing for the development of an axial force F; in the free-end condition, the end faces are fully stress-free so that $F = 0$, but allowing for the development of an axial displacement U uniform over the end face. It is noted that also in the free-end situation there is a distribution of axial stresses over a cross-section, but the resultant axial force vanishes.

The kinematics of the problem is readily established with the aid of a spatially fixed cylindrical coordinate system $x^i = (r, \theta, z)$ with associated orthonormal base vectors $\mathbf{e}_i$ (NEALE & SHRIVASTAVA [1990a,b]). These base vectors are associated with the current state, so that tensor components with respect to this basis represent physical components (notice that WU & VAN DER GIESSEN [1991] have used the same coordinate system, but have not normalized the associated base vectors). The deformations are assumed such that if the initial coordinates of a material point are $x_0^i = (r_0, \theta_0, z_0)$, its current coordinates are given by

$$r = r(r_0; t), \qquad \theta = \theta_0 + \omega(t)z_0, \qquad z = e(t)z_0,$$

with t a monotonic time-like parameter. Here, $\omega = \varphi/L_0$ is the twist per unit initial length of the bar and $e = L/L_0$ is the extensional stretch in axial direction. The velocity vector $\mathbf{v} = v_i\mathbf{e}_i$ is then given by

$$(v_i) = \left(\dot{r}, \frac{z\dot{\omega}}{e}, \frac{z\dot{e}}{e}\right),$$

and the components of $\mathbf{D} = D_{ij}\mathbf{e}_i \otimes \mathbf{e}_j$ and $\mathbf{W} = W_{ij}\mathbf{e}_i \otimes \mathbf{e}_j$ are obtained as

$$D_{11} = \frac{\partial \dot{r}}{\partial r}, \qquad D_{22} = \frac{\dot{r}}{r}, \qquad D_{33} = \frac{\dot{e}}{e}, \qquad D_{23} = \frac{1}{2}\frac{r\dot{\omega}}{e}, \qquad D_{12} = D_{13} = 0; \tag{27a}$$

$$W_{12} = -\frac{z\dot{\omega}}{e}, \qquad W_{13} = 0, \qquad W_{23} = \frac{1}{2}\frac{r\dot{\omega}}{e}. \tag{27b}$$

Due to axisymmetry and axial homogeneity, the stress components, $\boldsymbol{\sigma} = \sigma_{ij}\mathbf{e}_i \otimes \mathbf{e}_j$, satisfy $\sigma_{12} = \sigma_{13} = 0$ while $\sigma_{ij} = \sigma_{ij}(r; t)$ otherwise, taking into account the boundary condition $\sigma_{11}(R; t) \equiv 0$. The resultant torque T and the axial tensile force F are given by

$$T = 2\pi \int_0^R r^2 \sigma_{23}\, dr, \qquad F = 2\pi \int_0^R r\sigma_{33}\, dr. \tag{28}$$

For future reference, we define the shear at the outer radius of the bar measured in the initial undeformed configuration by

$$\Gamma = R_0\omega = \frac{R_0}{L_0}\varphi. \tag{29}$$

It is clear from the above considerations that the torsion problem is basically a one-dimensional problem along the radial coordinate r. In the case of torsion of an incompressible material under fixed-end conditions, this allows for a semianalytical approach to be discussed in the next section; in all other cases, one may rely on a numerical analysis which will be discussed in section III.3.

III.2. *Semianalytical method for fixed-end torsion of incompressible materials*

If the behavior is axisymmetric, axially homogeneous and incompressible, semianalytical solutions can be obtained for solid bars subjected to fixed-end torsion. This is possible since each material point is in this case simply loaded in simple shear under an additional hydrostatic pressure, where the shear γ is directly proportional to the radius r, $\gamma(r) = (r/R)\Gamma$ (note that now, $R \equiv R_0$). To apply this semianalytical method, we require the values of the deviatoric stress components $\mathbf{s}$ during simple shear as a function of the shear deformation γ, which is then readily translated into the stress deviator distribution $\mathbf{s}(r)$. To obtain the actual stress distribution $\boldsymbol{\sigma} = \mathbf{s} - p\mathbf{I}$, the hydrostatic pressure distribution $p(r)$ is needed (NEALE & SHRIVASTAVA [1990b]).

For the above conditions, the only equation of equilibrium which is not identically satisfied is the relation

$$r\frac{\partial \sigma_{11}}{\partial r} + \sigma_{11} - \sigma_{22} = 0.$$

This can be written in terms of p and the known $\mathbf{s}$ distribution as follows:

$$\frac{\partial p}{\partial r} = \frac{\partial s_{11}}{\partial r} + \frac{1}{r}(s_{11} - s_{22}). \tag{30}$$

Solving this numerically, together with the boundary condition $\sigma_{11}(R) = 0$, gives the hydrostatic pressure distribution $p(r)$. Combining this with the stress deviator distribution gives $\boldsymbol{\sigma}(r)$. The resultant torque and axial force are computed from (28).

For the constitutive models considered here we have $s_{11} = 0$, so that $\sigma_{11} = -p$. As a result, the boundary condition becomes $p(R) = 0$ and the solution to (30) reads

$$p(r) = -\int_R^r \frac{1}{r} s_{22}(\gamma)\, dr. \tag{31}$$

Since $s_{11} = 0$, we have $s_{33} = -s_{22}$ or $\sigma_{33} = -(s_{22} + p)$. Substituting this and (31) in (28b) and integrating by parts gives

$$F(\Gamma) = -\frac{3\pi R^2}{\Gamma^2} \int_0^\Gamma \gamma s_{22}(\gamma)\, d\gamma. \tag{32}$$

The expression (28a) for T can also be written as

$$T(\Gamma) = \frac{2\pi R^3}{\Gamma^3} \int_0^\Gamma \gamma^2 s_{23}(\gamma)\, d\gamma. \tag{33}$$

Thus, for a bar twisted to a shear deformation Γ at its outer radius, the simple shear solution $\mathbf{s}(\gamma)$ together with (32) and (33) immediately give the axial force and torque without having to solve explicitly for the pressure distribution $p(r)$. However, to obtain the corresponding stress distributions $\boldsymbol{\sigma}(r)$ across the bar, $p(r)$ must be determined by integrating (31).

III.3. *Finite element analysis*

A more versatile approach is a numerical analysis employing the finite elements illustrated in Fig. 2 (Wu & Van der Giessen [1991]). Each element is actually a circular cylindrical tube, but computationally it is considered to be one-dimensional along the r-axis, with two nodes at $r = r_1$ and $r = r_2$, respectively (see Fig. 2b). Within each element the radial velocity $v_1 = \dot{r}$ is interpolated through a linear interpolation of the cir-

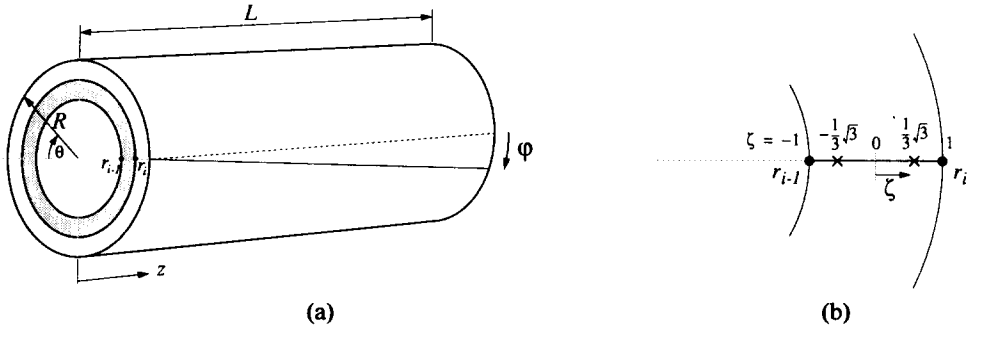

Fig. 2. (a) The special purpose finite element used for the analysis of torsion of bars with variable end conditions; (b) shows the nodal points (•) and the material sampling points (×) for each element.

cumferential strain-rate $D_{22} = \dot{r}/r$ between the nodal values $\dot{r}_1/r_1$ and $\dot{r}_2/r_2$. The degrees of freedom of the entire finite element model of the bar consisting of, say, n elements then comprise $n + 1$ radial nodal displacements along with the axial displacement U and the angle of twist φ. Within each element, two material sampling points or integration points are adopted. For more details concerning the precise formulation of the finite element equations, we refer to WU and VAN DER GIESSEN [1991]. The final governing equations are solved in a straightforward linear incremental fashion, which includes an equilibrium correction to prevent drifting of the solution away from the true equilibrium path. In integrating the constitutive equations for the stresses during the incremental process, the value of the parameter k to be used in (16) or (23) is at any increment adjusted such that the stress point remains on the yield surface exactly.

IV. RESULTS

IV.1. *Simple shear*

The primary deformation mode during torsion is simple shear. In fact, by taking $e = 1$ and $\dot{r} = 0$ and letting $\dot{\gamma} \equiv r\dot{\omega}$, the velocity gradient components in (27) reduce to $D_{23} = W_{23} = \dot{\gamma}/2$, $D_{ij} = 0$ otherwise, thus representing pure simple shear in the x_2-x_3 plane of a Cartesian frame of reference. As an introduction to the next sections on the full analysis of torsion of solid bars, we briefly consider here the response to simple shear according to the combined isotropic-kinematic hardening models of section II.2 in order to point out some basic characteristics of these models and to motivate the values of the material parameters used. A number of the features during simple shear carry over to the full torsion problem, so that we can use those in the discussion of the torsion results. All cases to be analysed here are for materials with a hardening exponent $N = 0.2$, Poisson's ratio $\nu = 0.49$, and $E/\sigma_y = 286$; thus, the elastic shear modulus $G = E/2(1 + \nu)$ is $G/\sigma_y = 96$ which will also be used in the forthcoming sections though with different Poisson's ratios.

Figure 3 shows the normalized shear stress response, σ_{23}/σ_y, as a function of the

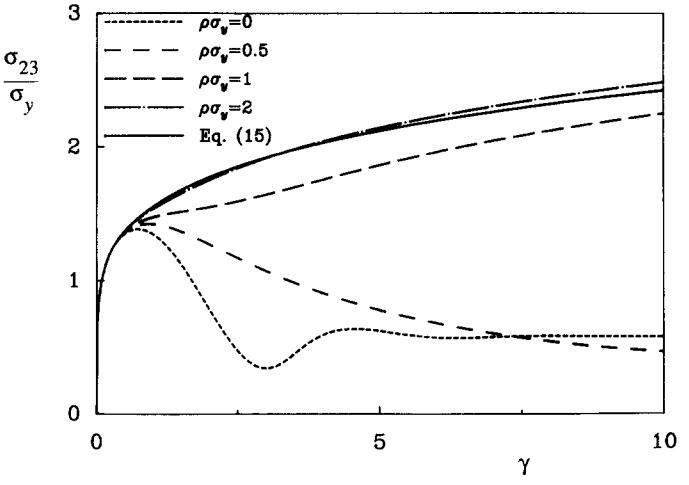

Fig. 3. Shear stress response during simple shear in the x_2-x_3 plane according to the DL model with pure kinematic hardening ($b = 0$).

shear γ for the DL model with pure kinematic hardening ($b = 0$) for various values of the plastic spin parameter ρ: either ρ is constant and takes values $\rho\sigma_y = 0$, 0.5, 1, 2, or ρ is taken to be given by the expression (15). As mentioned before, this kinematic hardening model reduces to the classical J_2 kinematic hardening model (TVERGAARD [1978]) for $\rho = 0$, and for that case Fig. 3 shows the oscillatory stress response for large strains observed first by NAGTEGAAL and DEJONG [1982]. For ρ according to (15) as suggested by PAULUN and PECHERSKI [1987b] or large values of ρ, for instance $\rho\sigma_y = 1$ or 2, the response is monotonic, and in fact deviates little from that for isotropic hardening ($b = 1$). For $\rho\sigma_y = 0.5$ there is not enough plastic spin and the shear stress response attains a maximum shortly after the first peak in the response for $\rho = 0$. It is noted here that the value of ρ necessary to obtain a monotonic response depends on the hardening characteristics; DAFALIAS [1985a] for instance found a monotonic response for values $\rho\sigma_y < 1$ using linear hardening ($E_t = \text{const.}$). Since a value $\rho\sigma_y = 2$ gives a response which is close that for ρ according to (15), we shall confine attention to the value $\rho\sigma_y = 1$ in the sequel.

In Fig. 4 we briefly consider the influence of the parameter b in the combined isotropic-kinematic hardening models of section II.2 on the shear stress response. Figures 4a and b both show results for the DL model with $\rho\sigma_y = 1$, but in Fig. 4a we have taken $\bar{\rho} = \rho$ independent of b, while in Fig. 4b we have used the b dependent scaling of $\bar{\rho}$ according to (14). In Fig. 4a we see that for small values of the shear strain, the shear stress varies with b between the purely kinematic response for $b = 0$ and the isotropic response for $b = 1$ in an almost linear fashion, as one would expect from the relationship (10). At large shears, however, this correlation has disappeared. As opposed to this, the linear variation of the response with b is maintained for all values of γ when using the modified expression for $\bar{\rho}$ as shown in Fig. 4b. It should be realized that both choices are rather arbitrary and that there is no physical reason to prefer one over the other; but, since the choice according to (14) gives a shear stress response which complies more to one's expectation in view of (10), this expression (14) is preferred for the present purpose. Using the assumption (15) for $\bar{\rho}$, the kinematic hardening results ($b = 0$) differ rather little from the isotropic hardening results ($b = 1$), and so do all intermediate cases; therefore, they are not shown. Hence, for $\bar{\rho}$ according to (15) there is little effect of anisotropic hardening on the shear stress response, but b does have a significant effect on the normal stress response, as will be discussed later. Figure 4c shows similar results but now for the VDG model. It is observed, first of all, that the response according to this model differs significantly from that for the DL model for all $b \neq 1$. These differences must be attributed to the different plastic spin constitutive laws involved. We also see that varying the value of b has a qualitatively similar effect to the response as in the case of Fig. 4a; but, it must be noted that in the VDG model there is no material parameter associated with the plastic spin to remedy this.

The constitutive models used here imply the development of normal stresses during simple shear; these stresses are the counterpart of the axial effects during torsion of solid bars to be discussed in the next sections. In Fig. 5 we briefly study the effect of b on the development of σ_{22}/σ_y (for the current models, $\sigma_{11} = 0$ and $\sigma_{33} = -\sigma_{22}$). Figure 5a shows results for the DL model with $\rho\sigma_y = 1$ and $\bar{\rho}$ according to (14). There is virtually no normal stress development in the case of isotropic hardening, while the response for pure kinematic hardening is strongly affected by the value of ρ, to the extent that the saturation value at large γ decreases with increasing ρ (cf. e.g. DAFALIAS [1985a]). It is noted that the response with $\bar{\rho}$ according to the expression (15) is rather similar but at a slightly lower stress level (at least for the parameter combination used here). For com-

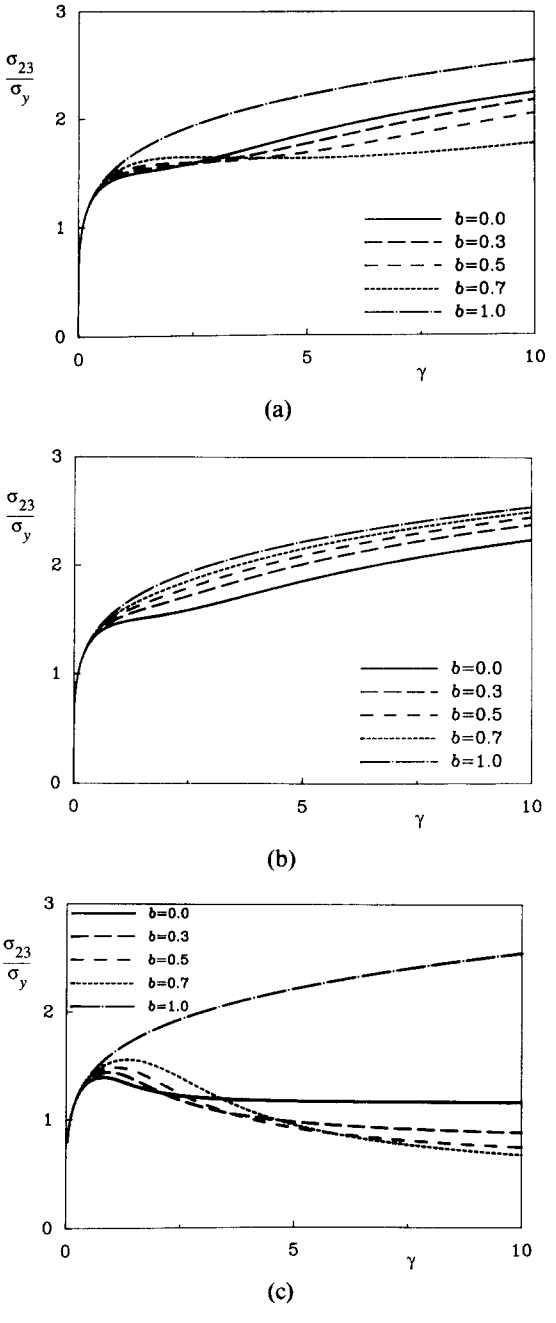

Fig. 4. Shear stress response during simple shear in the x_2-x_3 plane for combined isotropic-kinematic hardening with different values of b; (a) according to the DL model with $\bar{\rho} = \rho$; (b) according to the DL model with $\bar{\rho}$ according to (14); (c) according to the VDG model.

bined hardening, the response is in between those for kinematic and isotropic hardening. The normal stress development as predicted by the VDG model is shown in Fig. 5b. The important trend to be noted is the unbounded increase of the normal stress with increasing γ without saturation as found in Fig. 5a.

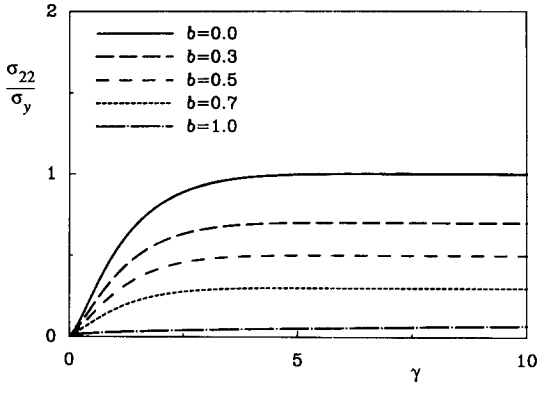

(a)

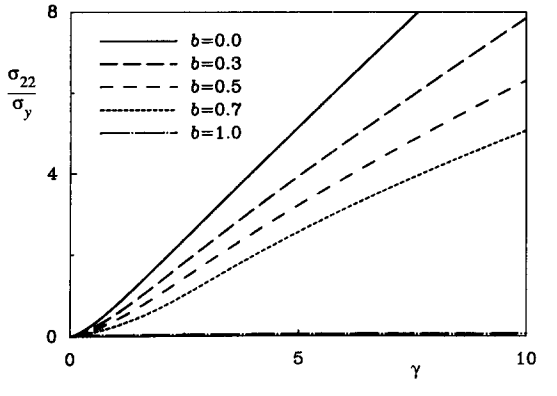

(b)

Fig. 5. Normal stress development during simple shear in the x_2–x_3 plane for combined isotropic-kinematic hardening with different values of b; (a) according to the DL model with $\rho\sigma_y = 1$; (b) according to the VDG model.

Some of the analyses have been repeated using the F2 model discussed in section II.3. Two versions of this model may be distinguished depending on whether the DL or the VDG formulation is used for the plastic spin in the kinematic hardening fraction. As shown in section II.3, the prediction of such models with ψ chosen equal to b coincides with that of the corresponding combined isotropic-kinematic hardening models of section II.2 in the case of uniaxial tension. Applying these models now to the simple shear problem, we find that when these models are based on the DL theory with $\bar{\rho}$ according to the expression (14), there is no longer a strict correspondence between the two predictions but the difference is quite small. However, when the models are based on the VDG theory, we find a considerable difference in the predicted shear stress responses for corresponding cases ($b = \psi$). It follows from the formulation of the F2 model that the response for any value of ψ is simply a corresponding linear combination of the response of a pure isotropic hardening and a pure kinematic hardening material. This agrees indeed with the linear variation of the response according to the combined isotropic-kinematic hardening DL model for different values of b (see Fig. 4b); but, this does not agree with the trends observed in Fig. 4c for the VDG model. So, on the basis of the VDG formulation of kinematic hardening, the F2 model and the combined hard-

ening model lead to two clearly different descriptions for shear (though their predictions coincide for uniaxial tension).

IV.2. *Fixed-end torsion*

In this section, we study the torsion of a solid bar made out of an incompressible material under fixed-end conditions. This corresponds to invoking the axial boundary conditions $\dot{e} = \dot{U} = 0$ in (27) and will lead to the development of an axial load F. This problem has been solved by the above finite element technique as well as by the semi-analytical method discussed in section III.2, which is feasible in this case owing to the assumed incompressibility. In the finite element analysis, elastic incompressibility is approximated by taking $\nu = 0.49$; some of the analyses have been repeated with $\nu = 0.499$ but the difference was insignificant. As in the previous section, the cases to be analysed in this section are for $N = 0.2$ and $G/\sigma_y = 96$. Having considered a variety of values of the parameter b in the previous section, we limit the analyses here to $b = 0$, 0.5, or 1. Also, in the DL model, we employ only a constant value of $\bar{\rho}$ according to (14) with $\rho\sigma_y = 1$ or take $\bar{\rho}$ to be given by the expression (15) as suggested by PAULUN & PECHERSKI [1987b].

The semi-analytical method [see (32)–(33)] has been based on the simple shear results presented in the previous section, using datasets with simple shear results for γ up to 10 at increments of $\Delta\gamma = 0.01$. The finite element analyses have used five elements, which was considered to be sufficient in previous investigations (WU & VAN DER GIESSEN [1991]) and which will be confirmed later on. Here and in the sequel, all torsion results are shown by way of plots of the torque T, normalized by $(\frac{2}{3})\pi\sigma_y R_0^3$, or the axial compressive force $-F$, normalized by $\pi\sigma_y R_0^2$, versus the shear Γ as defined in (29). Thus, the results are independent of the initial geometry of the bar, as is immediately clear from (28) and (29).

Figure 6a and b show the fixed-end torsion response for the DL model. Comparing with Fig. 4b, we see that the normalized T vs Γ plot for fixed-end torsion is very much akin to the normalized shear stress σ_{23} vs γ plots in pure simple shear. This was also found for cases with $\bar{\rho}$ according to (15), as well as for the VDG model, and had been observed for other constitutive models by NEALE and SHRIVASTAVA [1990a,b]. Qualitatively, the effect of anisotropic hardening, as specified in the present models by b, can therefore be readily deduced from the simple shear results presented in the previous section.

A similar correspondence between fixed-end torsion results and simple shear results is found when comparing the axial force response in Fig. 6b with the normal stress response ($-\sigma_{33} = \sigma_{22}$) to simple shear in Fig. 5a. The fact that saturation of F occurs at somewhat larger values of Γ than the saturation of σ_{22} as a function of γ must be attributed to the inhomogeneous axial stress distribution along the radius r. It is recalled (cf. section III.2) that the actual pressure distribution $p(r)$ was not needed in evaluating F from (32) using the semianalytical method.

In the results shown in Fig. 6, as well as in the other computations mentioned, we observe that the finite element solutions for the gross quantities F and Γ agree very well with the accurate semianalytical results. To further assess the accuracy of the finite element representation, we present the distributions of the axial stress $\sigma_{33} = -(s_{22} + p)$ and of the radial stress $\sigma_{11} = -p$ across the bar in Fig. 7. The semianalytical results are obtained by numerically solving (30). Results are given only for the extreme cases $b = 1$

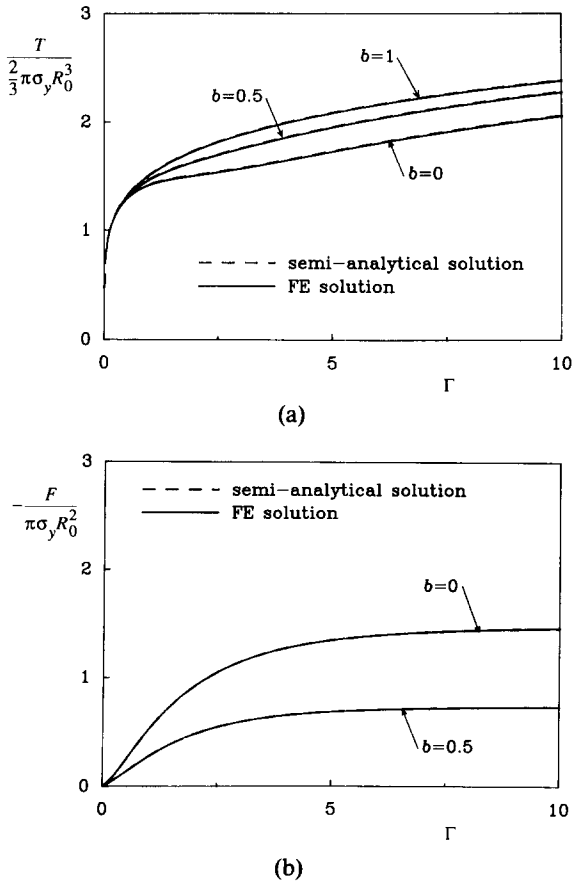

Fig. 6. Responses to fixed-end torsion according to the DL model with $\rho\sigma_y = 1$; (a) normalized torque; (b) compressive axial force.

and $b = 0$. The stress distributions according to the finite element solution are plotted by connecting the local values at the sampling points by straight lines. It is seen that the stress distributions are reasonably well captured by the finite element model, even though only five elements were used.

IV.3. *Free-end torsion*

We proceed by studying the torsion of the same bar as above, but under conditions of axially free ends. These conditions are obtained by imposing the opposite axial boundary condition as in the previous case of fixed-end torsion, i.e. $F = 0$ in (28), thus allowing for an axial strain e. The analyses have been carried out numerically using five torsion elements as before. The material was taken to be characterized by $N = 0.2$ and $G/\sigma_y = 96$ just as in the previous sections; but, the Poisson ratio was taken here as $\nu = 0.3$, which is more realistic for metals, so that $E/\sigma_y = 250$ (it is noted however that the results to be presented are only weakly sensitive to the value of ν as discussed also by WU & VAN DER GIESSEN [1991]).

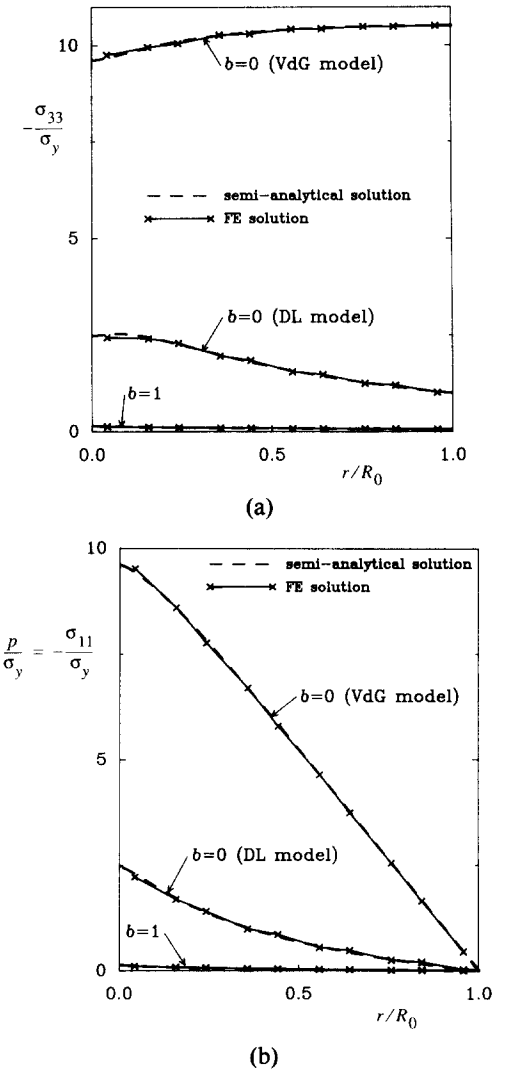

Fig. 7. Stress distributions across the bar during fixed-end torsion according to the DL model with $\rho\sigma_y = 1$ and according to the VDG model; (a) axial stress σ_{33}; (b) stress σ_{11}, or pressure p.

Figures 8–10 present the torque response and the accompanying axial strain development during free-end torsion. As in the case of fixed-end torsion, the torque T is normalized by the constant $(\frac{2}{3})\pi\sigma_y R_0^3$ and results are plotted versus the parameter Γ, both being determined by the initial geometry of the bar. It should be noted that the axial strain predicted by all considered models, which for some cases can be quite substantial, is accompanied by radial and circumferential strains of the same order of magnitude, since the dilatation results from elastic strains only. Thus, Γ will generally not be an accurate measure of the actual shear strain at the current radius of the bar.

In Fig. 8 the effect of different plastic spin constitutive laws on the torque response is shown. Figure 8a shows results for the DL model with $\rho\sigma_y = 1$ and $\bar{\rho}$ evaluated according to (14) for different values of b. Comparing with the torque predictions for

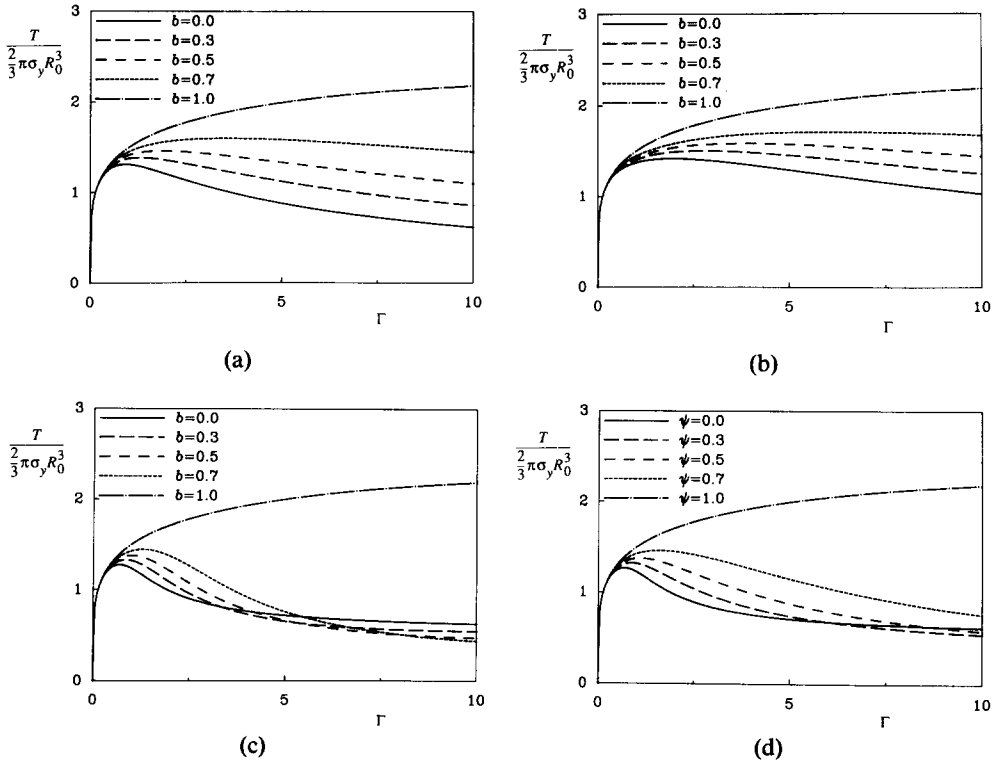

Fig. 8. Normalized torque responses in free-end torsion; (a) according to the DL model with $\rho\sigma_y = 1$; (b) as in (a) but with $\bar{\rho}$ according to (15); (c) according to the VDG model; (d) according to the F2 model based on the VDG kinematic hardening theory.

fixed-end torsion in Fig. 6a, it is seen that the difference between predictions for $b = 1$ (isotropic hardening) and $b = 0$ (kinematic hardening) is much larger in free-end torsion. The torque predictions with $b = 1$ for fixed and free-end torsion are found to differ little (less than 10% at $\Gamma = 10$). For $b = 0$, a maximum in the torque response at $\Gamma = 0.9$ is predicted for this model, while the torque during fixed-end torsion increased monotonically. A similar sensitivity for the amount of anisotropic hardening is observed in Fig. 8b for again the DL model, but with $\bar{\rho}$ according to (15). In contrast, b was found to have only little influence on the torque response during fixed-end torsion, as discussed above. Again for $b = 0$, the torque reaches a maximum in free-end torsion but at a later stage, $\Gamma = 2$. It is noted that the results for $\rho\sigma_y = 2$ are close to these results for $\bar{\rho}$ according to (15), just as was found above in simple shear. The same tendency in the dependence on b is observed when using the VDG model as shown in Fig. 8c. In Fig. 8d, finally, results are shown for the F2 model based on the VDG formulation. As discussed in the previous section, the predicted torque response during fixed-end torsion for any value of ψ is a linear combination of the response of a pure isotropic hardening and a pure kinematic hardening material. This character of the solution is retained in free-end torsion in the early stages, say up to $\Gamma \approx 2$, but is essentially lost for large twists.

Figure 9 shows the axial strain e as predicted by some of the constitutive models for a chosen amount of anisotropic hardening specified by either $b = 0.5$ or $\psi = 0.5$ in the

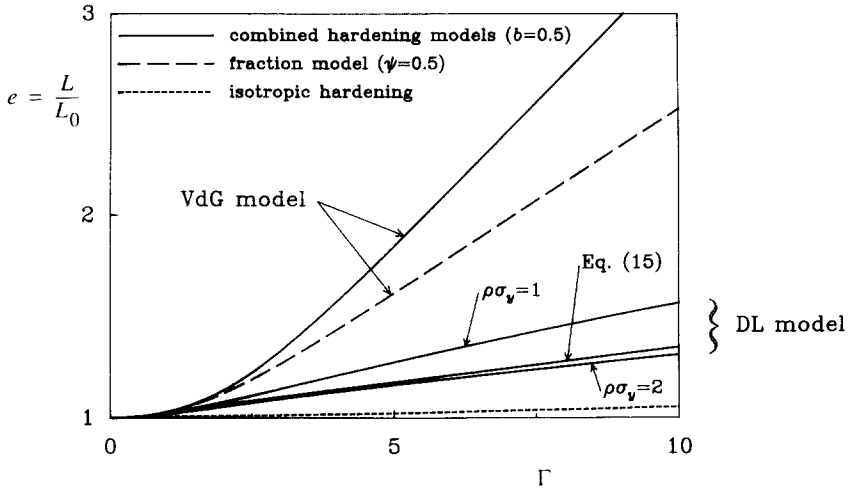

Fig. 9. Axial strain development during free-end torsion according to various combined isotropic-kinematic hardening models with $b = 0.5$ or $\psi = 0.5$.

case of the two-fraction model. The result according to the isotropic hardening model is shown for comparison. As expected from the predicted axial forces during fixed-end torsion in the previous section, the precise formulation of the plastic spin constitutive law has an important effect on the axial strain development during free-end torsion. For the values of $\bar{\rho}$ considered here, the DL model tends to predict smaller axial strains than the corresponding VDG model. In the case of the DL model with constant values of ρ, the predicted axial effect decreases significantly with increasing value of ρ. It is also interesting to note that the axial strain predicted by this model keeps increasing within the twist range considered, whereas the axial force during fixed-end torsion

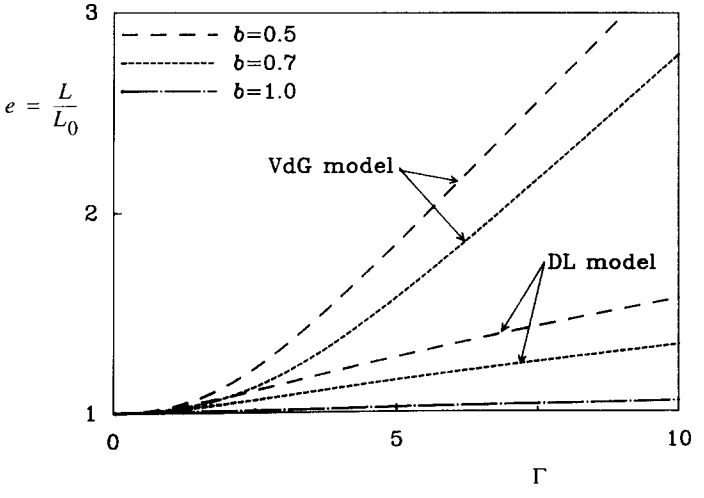

Fig. 10. Axial strain during free-end torsion according to the VDG model and the DL model with $\bar{\rho}$ according to (14) and $\rho\sigma_y = 1$, for various values of b.

showed saturation. Figure 9 also shows that the combined hardening model of section II.2 and the F2 model of section II.3, both based on the VDG formulation of the plastic spin (and, therefore, equivalent in uniaxial tension), lead to significantly different predictions of the axial effect. The F2 model based on the DL formulation also predicts different axial strains than those shown in Fig. 9 for equal values of b and ψ, but to a much lesser extent. In Fig. 10 we summarize the effect of the amount of anisotropic hardening in the combined models, as specified by b, on the axial strain development during free end torsion.

It is of interest now to gain some insight into the evolution of plastic spinning during free-end torsion in comparison with that during fixed-end torsion. To that end we consider the value of the only nonvanishing component of $\mathbf{W}^p$, namely W_{23}^p, at the outer radius of the bar in reference to the continuum spin W_{23} (note that the ratio W_{23}^p/W_{23} is equal to the corresponding ratio of physical components). The plastic spin during fixed-end torsion is governed completely by the plastic spinning during simple shear which has been discussed in some detail by VAN DER GIESSEN [1991]. The general tendency of his results is that for the pure kinematic hardening versions ($b = 0$) of the constitutive models considered here, there is a more or less gradual S-shaped transition from $W_{23}^p = 0$ initially to a value equal to the applied spin W_{23} at large shears, provided that ρ is sufficiently large in the DL model (the value $\rho\sigma_y = 1$ was found to satisfy here). Results for mixed hardening are not plotted here, but they show that for $\bar{\rho}$ according to (14) the plastic spin is virtually insensitive to b, while there is only a slight effect for $\bar{\rho}$ according to (15). For the VDG model, the transition from $W_{23}^p = 0$ to $W_{23}^p = W_{23}$ is shifted to larger shears with increasing b. In Fig. 11 we now show the development of the plastic spin component W_{23}^p normalized by the continuum spin W_{23}, eqn (27b), at the outer radius of the bar as predicted for free-end torsion. The plastic spin at the outer radius is computed from the values at the two sampling points of the outermost finite element by extrapolation. Figures 11a and b show results for the DL model for different values of b with $\rho\sigma_y = 1$ and $\bar{\rho}$ evaluated according to (14) and $\bar{\rho}$ according to (15), respectively. Comparing with simple shear results (VAN DER GIESSEN [1991]), it is seen that while the plastic spin in simple shear was virtually insensitive to b when $\bar{\rho}$ according to (14) was used, it is significantly dependent on b during free-end torsion when $\Gamma > 2$ roughly. A second important feature is that during free-end torsion we no longer find the typical S-shaped transition from $W_{23}^p = 0$ to $W_{23}^p = W_{23}$. Instead, the transition tends to be terminated after some twist and the plastic spin starts to slowly drop with ongoing twist. The maximum value of the plastic spin attained is seen to depend on the value of $\bar{\rho}$ as well as on b, with the peak value increasing with increasing b (corresponding to a decreasing contribution of kinematic hardening). In the case of $\bar{\rho}$ according to (15), there is a tendency for larger values of b to develop a distinct peak in W_{23}^p which may exceed W_{23}. The drop in plastic spinning at somewhat larger twists is also predicted by the VDG combined hardening model, see Fig. 11c; but the effect of b is now different. Figure 11d finally shows the average plastic spin component $\overline{W}_{23}^p$, eqn (16), according to the F2 model based on the VDG plastic spin constitutive law. It is seen that the plastic spin predictions of this model are quite different from the predictions of the corresponding VDG combined hardening model shown in Fig. 11c. One may notice that the general tendency of the effect of ψ is similar to the effect of b in the results of Fig. 11a.

The F2 model considered in the foregoing is a particular example of two-fraction models, in which the material parameters were chosen equal for the isotropic hardening fraction and for the kinematic hardening fraction. As discussed in section II.3, this choice

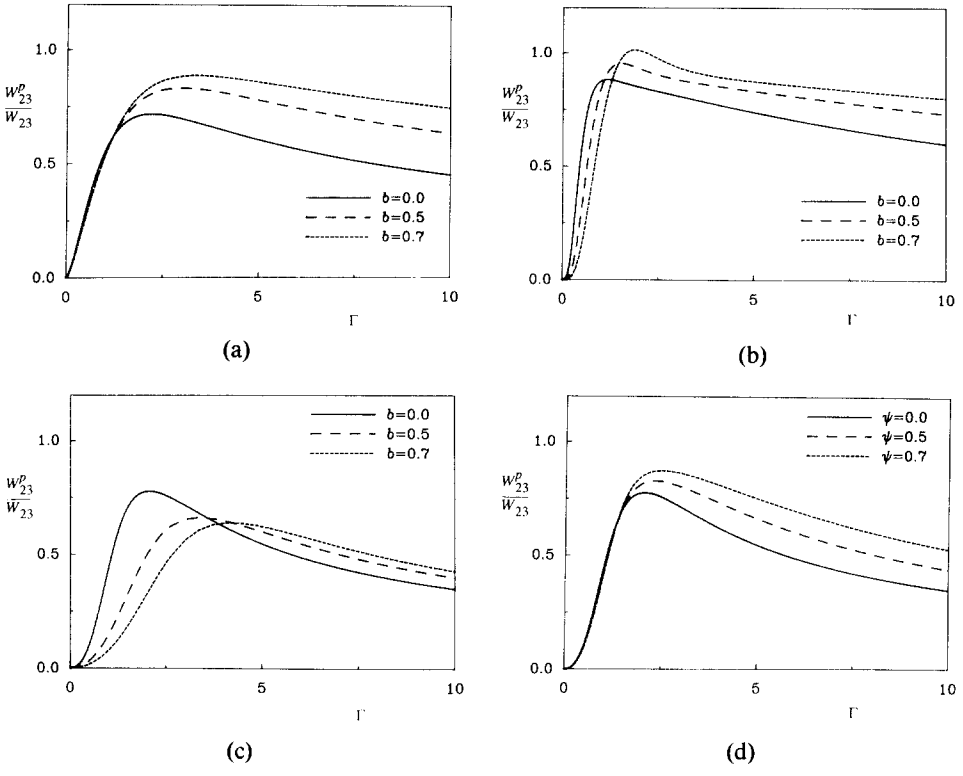

Fig. 11. Normalized plastic spin at outer radius of bar during free-end torsion; (a) according to the DL model with $\rho\sigma_y = 1$; (b) as in (a) but with $\bar{\rho}$ according to (15); (c) according to the VDG model; (d) according to the F2 model based on the VDG kinematic hardening theory.

was made so as to provide an alternative to the combined hardening models developed in section II.2. It was also mentioned that the fraction concept allows for more versatile constitutive models. An apparent first extension of the F2 model would be to allow for different hardening characteristics. For the purpose of illustration, Fig. 12 shows the torque response as predicted by such a model based on the VDG plastic spin constitutive law when the strain hardening exponent for the kinematic hardening fraction has been lowered to $N = 0.05$. The effect of this change is clear from comparison with the results of the F2 model in Fig. 8d. As expected, the axial strain e predicted by this fraction model is considerably smaller ($e = 1.6$ at $\Gamma = 10$ for $\psi = 0.5$) than that according to the F2 model (cf. Figure 9) since the contribution of kinematic hardening is less.

V. DISCUSSION AND CONCLUSION

In this article we have analysed the large strain torsion of solid circular bars under fixed-end as well as free-end conditions using a numerical method based on simple, special purpose finite elements. Assuming incompressible behavior it was also possible to analyse fixed-end torsion with the semianalytical method developed by NEALE and SHRIVASTAVA [1990a,b]. Detailed comparisons have been carried out which reveal that, with only five elements, very accurate results are obtained for gross quantities like torque and axial force as well as for the stress distributions across the specimen.

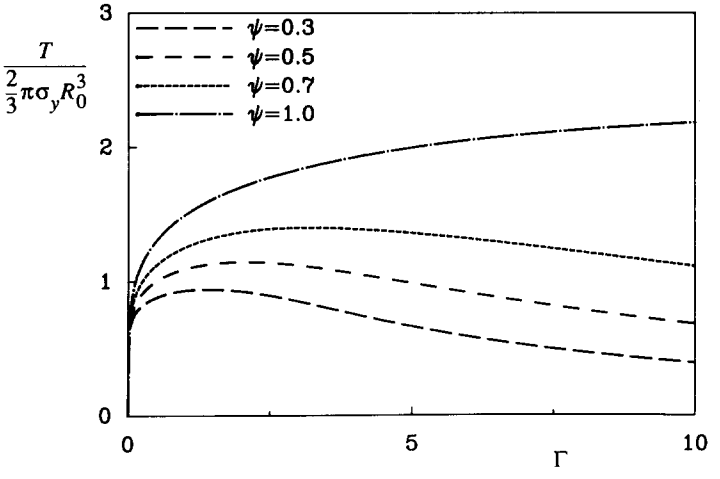

Fig. 12. Normalized torque responses in free-end torsion according to two-fraction model with one isotropic fraction ($N = 0.2$) and one kinematic hardening fraction ($N = 0.05$) based on the VDG theory.

The analyses have used various constitutive equations for combined isotropic-kinematic hardening based on different constitutive assumptions for the plastic spin. The constitutive models have been designed to yield identical descriptions for uniaxial tension in which case the plastic spin vanishes. Comparing the original proposals of the plastic spin laws for kinematic hardening (DAFALIAS [1983,1985a,b]; LORET [1983]; PAULUN & PECHERSKI [1987b]; VAN DER GIESSEN [1989b]) it becomes clear that the predicted responses to large simple shear are sensitive to the type of plastic spin law used as well as to the value of the material parameter ρ in the DL constitutive law of DAFALIAS [1985a] and LORET [1983]. This sensitivity is confirmed here within the more general class of combined hardening models. By virtue of the direct correspondence with simple shear, the torsion of a solid bar of an incompressible material with fixed ends, and in particular the associated axial force, is readily found to depend strongly on the plastic spin law. Our analyses show, furthermore, that this dependence as for the torque response is even more pronounced in the case of free-end torsion. Nevertheless, we can conclude that the basic trend in the axial strain development is qualitatively similar for each of the models: initially the axial elongation increases quadratically with the angle of twist while for larger shears, $\Gamma > 5$ roughly, the axial strain increase is almost linear with twist (at least up to $\Gamma = 10$). It is noted in passing that this behavior is affected by the type of strain hardening (see WU & VAN DER GIESSEN [1991]). Quantitatively, the results depend on the plastic spin constitutive law, where the VDG model tends to predict larger axial effects than the DL model.

It has been suggested on occasions (e.g. NEALE & SHRIVASTAVA [1990b]) that the development of axial force during fixed-end torsion will be fully analogous to the development of axial strain during free-end torsion. However, the present analyses of both processes have shown that this is not generally true. For instance, when applying the DL model with sufficiently large values of $\bar{\rho}$ the axial strain during free-end torsion continues to grow within the twist range considered ($\Gamma \leq 10$), whereas the axial force during fixed-end torsion showed saturation (at a $\bar{\rho}$-dependent value) after $\Gamma \approx 5$. This must be attributed to the path history dependence of such models along with the inhomogeneous

stress distributions across the bar. This observation demands due care in interpreting normal stress development during simple shear in terms of axial elongations in free-end torsion of solid bars, or vice versa. It has also been found that the torque responses in fixed and free-end torsion differ considerably, except in the case of isotropic hardening where they are roughly the same. This can, at least partly, be explained from the appreciable change in radius of the bar during free-end torsion as a result of the lengthening of the bar, but will also be due to the different stress histories.

It seems opportune to include here a brief discussion of some available experimental results that include axial effects. SWIFT [1947] appears to have been the first to conduct free-end torsion tests up to large strains (of the order of $\Gamma = 6$). Solid circular bars as well as tubes of several metals (brass 70:30, stainless-steel, aluminum, cupro-nickel, copper, mild steel, 0.5%C steel, lead) were used and, with the exception of lead specimens, all specimens exhibited monotonic lengthening. The length increase with twist exhibited a near-parabolic behavior initially, followed by a more or less steady rate of stretching for most materials (e.g. brass and stainless-steel), much like the responses obtained here. For copper a final transition to a lower rate of lengthening was observed at large shears. The total elongation depended on the material, with a maximum of $e \approx 1.12$ for brass at $\Gamma \approx 5$. Recent free-end experiments by DELHAGE [1990] on stainless-steel 304 have basically confirmed SWIFT's [1947] results. Regarding the torque response during free-end torsion, these experiments showed that for all materials considered the torque increased monotonically with continued twisting and that there was very little Bauschinger effect observed upon reversal of the twisting direction. Fixed-end torsion of solid bars (aluminum, copper, iron) was reported by MONTHEILLET *et al.* [1984]. At room temperature, an axial compressive force was found in all cases which increased linearly up to failure in the case of iron, but attained a maximum at shears of the order 1 to 2 for copper and aluminum; in the latter case, a decrease of the axial force was observed until a minimum was reached around $\Gamma \approx 3$ followed by an almost linear increase up to failure. At elevated temperatures, the behavior became even more complex due to additional thermally activated phenomena which are outside the scope of this study. Torque–twist curves were only presented by MONTHEILLET *et al.* [1984] for elevated temperatures. The common characteristic is the attainment of a single maximum at a relatively small shear; but, the torque response is likely to be monotonic with the angle of twist at ambient temperatures.

A qualitative comparison of these experimental results (at room temperature) with the predictions of the constitutive models considered here reveals that the experimentally observed monotonic torque–twist curve in fixed as well as free-end torsion can be simulated by all models provided a value b close to unity is used, corresponding to a small degree of kinematic hardening. This is in keeping with the fact that the experiments show only a small Bauschinger effect. The torque behavior in the fixed-end torsion results of MONTHEILLET *et al.* [1984] at elevated temperatures is reminiscent of the VDG model predictions for somewhat smaller values of b (cf. the simple shear results in Fig. 4c), but it should be realized that in fact all models considered here do not apply in that temperature range. As for the axial effects, it is seen that the monotonic lengthening during free-end torsion can be simulated qualitatively by all of the models considered, but the final decline in the lengthening rate exhibited by copper is not predicted by any of them. Also, the rather complex behavior of the axial compressive force during fixed-end torsion of copper and aluminum specimens mentioned above cannot be described by any of these models. It will be noted however that, since our aim was to focus on the effect of plastic spin, we have considered a rather limited subset of the class of combined isotropic-kinematic hardening models. In particular, we feel that the assumption

made here of a constant value of b, i.e. a constant ratio between isotropic hardening and kinematic hardening contributions, may have an important effect on the predictive capabilities of this class of models. A comparison of our present predictions and the experimental results suggests that the application of variable, history dependent values of b, so that b can be taken to vary from relatively small values at small strains to values close to unity at large strains, could improve the predictions considerably. Other improvements could possibly result from recent extensions of this class of constitutive models by, e.g., SHI *et al.* [1990]. Further investigation of these aspects in quantitative comparison with experimental results is currently in progress (see, e.g., VAN DER GIESSEN *et al.* [1991]).

As mentioned before, it has been established (e.g. GIL-SEVILLANO *et al.* [1975]; MONTHEILLET *et al.* [1984]; HARREN *et al.* [1989]) that the Swift effect is due to the development of texture in the polycrystalline aggregate. As in all other related phenomenological works known to us, it has been attempted to describe the associated deformation-induced anisotropy by including a kinematic hardening component in the hardening response. In fact, the plastic spin discussed here is directly proportional to the tensor kinematic variable. On the other hand, as pointed out already by MANDEL [1971], the micromechanics of crystallographic texture development relates the macroscopic plastic spin in a polycrystalline material to crystallographic slip. On the basis of this discrepancy one may question if a kinematic hardening related plastic spin constitutive law is appropriate for modeling this kind of deformation-induced anisotropy. These and related issues are discussed in some detail in VAN DER GIESSEN [1991] and are the subject of work in progress.

A final related point is the plastic spin at the outer radius of the bar during free-end torsion which, for all models considered here, shows a tendency to decline after a certain amount of twist. It is interesting to compare this with recent micromechanical analyses of VAN DER GIESSEN and VAN HOUTTE [1991], who computed the average plastic spin associated with crystallographic texture development from a Taylor polycrystal model. This average plastic spin found during simple shear agrees well qualitatively with the present phenomenological predictions. VAN DER GIESSEN and VAN HOUTTE [1991] also studied simple shear with simultaneous plane strain extension in the direction perpendicular to the shear plane; this deformation process bears some similarity to the deformation pattern at the outer radius of a bar loaded in free-end torsion with significant axial straining. The interesting conclusion now appears from their micromechanical analysis that the plastic spin also shows the typical S-curve type of development as a function of shear as in simple shear; moreover, the transition is found to be accelerated by simultaneous extension. Evidently, this kind of behavior is not reproduced by the present constitutive models. It is therefore concluded that more research is necessary which aims at providing physically sound realistic constitutive laws for the plastic spin.

Acknowledgements—The work of E. Van der Giessen was made possible by a fellowship of the Royal Netherlands Academy of Arts and Sciences.

REFERENCES

1947 SWIFT, H.W., "Length Changes in Metals Under Torsional Overstrain," Engineering, **163**, 253.
1958 BESSELING, J.F., "A Theory of Elastic, Plastic and Creep Deformations of an Initially Isotropic Material," J. Appl. Mech., **25**, 529.
1958 HILL, R., "A General Theorem of Uniqueness and Stability in Elastic Plastic Solids," J. Mech. Phys. Solids, **6**, 236.

1971 MANDEL, J., "Plasticité Classique et Viscoplasticité," CISM Lecture Notes No. 97, Udine, Springer-Verlag, Berlin.
1975 GIL-SEVILLANO, J., VAN HOUTTE, P., and AERNOUDT, E., "Deutung der Schertexturen mit Hilfe der Taylor-Analyse," Z. Metallkunde, **66**, 367.
1978 TVERGAARD, V., "Effect of Kinematic Hardening on Localized Necking in Biaxially Stretched Sheets," Int. J. Mech. Sci., **20**, 651.
1982 NAGTEGAAL, J.C., and DEJONG, J.E., "Some Aspects of Nonisotropic Work Hardening in Finite Strain Plasticity," in LEE, E.H., and MALLETT, R.L. (eds.), Plasticity of Metals at Finite Strain: Theory, Computation and Experiment, Stanford University/RPI, pp. 65–102.
1983 DAFALIAS, Y.F., "Corotational Rates for Kinematic Hardening at Large Plastic Deformation," J. Appl. Mech., **50**, 561.
1983 LORET, B., "On the Effects of Plastic Rotation in the Finite Deformation of Anisotropic Elastoplastic Materials," Mech. Mater., **2**, 287.
1984 MONTHEILLET, F., COHEN, M., and JONAS, J.J., "Axial Stresses and Texture Development During the Torsion Testing of Al, Cu and α-Fe," Acta Metall., **32**, 2077.
1985 BESSELING, J.F., "Models of Metal Plasticity: Theory and Experiment," in SAWCZUK, A., and BIANCHI, G. (eds.), Plasticity Today: Modelling, Methods and Applications, Elsevier, New York, pp. 97–113.
1985a DAFALIAS, Y.F., "A Missing Link in the Macroscopic Constitutive Formulation of Large Plastic Deformations," in SAWCZUK, A., and BIANCHI, G. (eds.), Plasticity Today: Modelling, Methods and Applications, Elsevier, New York, pp. 135–151.
1985b DAFALIAS, Y.F., "The Plastic Spin," J. Appl. Mech., **52**, 865.
1985 MEAR, M.E., and HUTCHINSON, J.W., "Influence of Yield Surface Curvature on Flow Localization in Dilatant Plasticity," Mech. Mater., **4**, 395.
1985 NEALE, K.W., and SHRIVASTAVA, S.C., "Finite Elastic-Plastic Torsion of a Circular Bar," Engng. Fracture Mech., **21**, 747.
1985 VAN DER GIESSEN, E., "Large Continuum Deformation Processes and Appropriate Models of Plasticity," Delft University of Technology, Laboratory for Engineering, mech. rep. no. 811.
1986 HUETINK, H., "On the Simulation of Thermomechanical Forming Processes," Ph.D. dissertation, Twente University, Enschede.
1987 AIFANTIS, E.C., "The Physics of Plastic Deformation," Int. J. Plast., **3**, 211.
1987 DAFALIAS, Y.F., "Issues on the Constitutive Formulation at Large Elastoplastic Deformations, Part 1: Kinematics," Acta Mech., **69**, 119.
1987a PAULUN, J.E., and PECHERSKI, R.B., "On the Application of the Plastic Spin Concept for the Description of Anisotropic Hardening in Finite Deformation Plasticity," Int. J. Plasticity, **3**, 303.
1987b PAULUN, J.E., and PECHERSKI, R.B., "Remarks on the Description of Anisotropic Hardening in Finite Deformation Plasticity," Arch. Mech. (to appear).
1988 LIPKIN, J., CHIESA, M.L., and BAMMANN, D.J., "Thermal Softening of 304L Stainless Steel: Experimental Results and Numerical Simulations," in CHIEM, C.Y., KUNZE, H.-D., and MEYER, L.W. (eds.), Impact Loading and Dynamic Behavior of Materials, DGM, Oberursel (FRG), pp. 687–694.
1988 ZBIB, H.M., and AIFANTIS, E.C., "On the Concept of Relative and Plastic Spins and its Implications to Large Deformation Theories. Part II: Anisotropic Hardening Plasticity," Acta Mech., **75**, 35.
1989 HARREN, S., LOWE, T.C., ASARO, R.J., and NEEDLEMAN, A., "Analysis of Large-Strain Shear in Rate-Dependent Face-Centred Cubic Polycrystals: Correlation of Micro- and Macromechanics," Phil. Trans. R. Soc. Lond., **A328**, 443.
1989a VAN DER GIESSEN, E., "Continuum Models of Large Deformation Plasticity—Part I: Large Deformation Plasticity and the Concept of a Natural Reference State," Eur. J. Mech. A/Solids, **8**, 15.
1989b VAN DER GIESSEN, E., "Continuum Models of Large Deformation Plasticity—Part II: A Kinematic Hardening Model and the Concept of a Plastically Induced Orientational Structure," Eur. J. Mech. A/Solids, **8**, 89.
1990 DELHAGE, L., "Strain-Rate and Axial Effects During Reversed Large Strain Torsion of Solid Circular Bars," Delft University, mech. rep. no. 924.
1990a NEALE, K.W., and SHRIVASTAVA, S.C., "Kinematic Work Hardening Models and Their Implications for Large Strain Plastic Behaviour in Torsion," in BOEHLER, J.P., (ed.), Yielding, Damage and Failure of Anisotropic Solids, Mechanical Engineering Publishers, London, pp. 131–143.
1990b NEALE, K.W., and SHRIVASTAVA, S.C., "Analytical Solutions for Circular Bars Subjected to Large Strain Plastic Torsion," J. Appl. Mech., **57**, 298.
1990 SHI, M.F., GERDEEN, J.C., and AIFANTIS, E.C., "On Finite Deformation Plasticity With Directional Softening. Part I: One-Component Model," Acta Mech., **83**, 103.
1990 VAN DER GIESSEN, E., "A Model of Anisotropically Hardening Materials Based Upon the Concept of a Plastically Induced Orientational Structure," in BOEHLER, J.P. (ed.), Yielding, Damage and Failure of Anisotropic Solids, Mechanical Engineering Publishers, London, pp. 187–198.
1991 TVERGAARD, V., and VAN DER GIESSEN, E., "Effect of Plastic Spin on Localization Predictions for a Porous Ductile Material," J. Mech. Phys. Solids, **39**, 763.

1991 VAN DER GIESSEN, E., "Micromechanical and Thermodynamic Aspects of the Plastic Spin," Int. J. Plasticity, **7**, 365.

1991 VAN DER GIESSEN, E., and VAN HOUTTE, P., "A Study of the Macroscopic Plastic Spin in Polycrystals," in JONO, M., and INOUE, T. (eds.), Mechanical Behaviour of Materials—VI, Vol. 1, Pergamon, Oxford, pp. 99–104.

1991 VAN DER GIESSEN, E., WU, P.D., and HEALE, K.W., "Effect of Plastic Spin and Deformation-Induced Anisotropy on Large Strain Torsion of Solid Bars," in Proc. of IUTAM symposium on 'Constitutive Relations for Finite Deformation of Polycrystalline Metals," July 1991, Beijing, China (to appear).

1991 WU, P.D., and VAN DER GIESSEN, E., "Analysis of Elastic-Plastic Torsion of Circular Bars at Large Strains," Arch. Appl. Mech. (Ingenieur-Archiv), **61**, 89.

Delft University of Technology
Laboratory for Engineering Mechanics
P.O. Box 5033, 2600 GA Delft, The Netherlands

China University of Mining and Technology
Beijing Graduate School
Beijing, China

Université de Sherbrooke
Fac. des Sciences Appliquées
Sherbrooke, Quebec J1K 2R1, Canada

(*Received* 19 *April* 1991; *in final revised form* 3 *January* 1992)